Sensitivity of total column ozone to stratospheric sulfur injection strategies

S. Tilmes[1], J. H. Richter[2], B. Kravitz[3,4], D. G. MacMartin[5], A. S. Glanville[2], D. Visioni[5], D. E. Kinnison[1], R. Müller[6]

[1]Atmospheric Chemistry, Observations, and Modeling Laboratory, National Center for Atmospheric Research, Boulder CO, USA

[2]Climate and Global Dynamics Laboratory, National Center for Atmospheric Research, Boulder CO, USA

[3]Department of Earth and Atmospheric Sciences, Indiana University, IN, USA

[4]Atmospheric Sciences and Global Change Division, Pacific Northwest National Laboratory, Richland, WA, USA

[5]Mechanical and Aerospace Engineering, Cornell University, Ithaca, NY, USA

[6]Research Center Jülich, Jülich, Germany

Key Points:

- Onset of stratospheric sulfur injection results in an abrupt deepening of the ozone hole in the first 10 years
- The ozone hole recovers fastest with low-altitude injections and slowest with equatorial injections
- Stratospheric sulfur injection can lead to an increase in column ozone in tropics and mid-latitudes

Corresponding author: Simone Tilmes, `tilmes@ucar.edu`

Abstract

Stratospheric sulfur injection at multiple locations, to counter greenhouse gas induced warming, may reduce some of the side effects of stratospheric aerosol interventions. We explore the impact of different injection strategies on total column ozone (TCO) using two configurations of a fully coupled Earth system model. The discussed experiments maintain global surface temperatures at 2020 conditions, while following the unmitigated RCP8.5 future scenario. Within the first ten years of the injection, we find an abrupt deepening of the Antarctic ozone hole by 8–20% and changes up to ±5% for other regions and seasons. Dependent on the injection strategy, the recovery of the Antarctic ozone hole to 1980 conditions is delayed by ≈25 to over 55 years. Mid to high-latitude TCO increases by ≈15% in Northern Hemisphere winter and spring between 2010–2019 and 2080–2089 due to both, increasing greenhouse gases and increasing sulfur injections. Implications for ecosystems need to be investigated.

1 Introduction

Climate intervention strategies using stratospheric sulfate aerosols to counter the surface warming caused by increasing greenhouse gases, have been shown to impact stratospheric ozone, as discussed in various studies [e.g., *Tilmes et al.*, 2008; *Rasch et al.*, 2008; *Heckendorn et al.*, 2009; *Tilmes et al.*, 2012; *Xia et al.*, 2017; *Tilmes et al.*, 2018a]. In many of these studies, a fixed amount of sulfur injections has been applied within a year and injections were maintained for a continuous period of time. Furthermore, earlier studies prescribed fixed stratospheric aerosol distributions or varying distributions that were based on tropical injections only. The enhanced stratospheric sulfate burden results for instance in a reduction of total column ozone (TCO) over Antarctica during the ozone hole period through increased chlorine and bromine activation, promoting catalytic ozone-destroying cycles. The start of sulfur injections has been usually chosen around present day, a time when the stratospheric halogen loading is high. Therefore, a question remains to be answered: At what point has the stratospheric halogen loading declined sufficiently to minimize these effects?

In recent years, strategic climate intervention modeling experiments have been designed to keep future surface temperatures from changing compared to 2020 conditions, while following different greenhouse forcing scenarios [*Kravitz et al.*, 2017; *Richter et al.*, 2017; *Tilmes et al.*, 2018a, 2020]. In particular, these studies used a feedback control al-

gorithm to identify the required sulfur injection amounts at four stratospheric point locations at 30°N and 30°S and 15°N and 15°S in latitude, 180°W in longitude, and at about 6 km above the tropopause in altitude. Annually varying injection amounts at those locations were adjusted to keep global, as well as interhemispheric and pole-to-Equator surface temperature gradients from changing [e.g., *MacMartin et al.*, 2017]. In contrast to many earlier studies, the geoengineering large ensemble (GLENS) simulations [*Tilmes et al.*, 2018b] gradually and continuously increased sulfur injections starting in 2020, in order to keep surface temperatures at 2020 levels while following the RCP8.5 scenario. Similarly, a gradual increase of stratospheric sulfur injections was applied for the so called "peak-shaving" experiments [*Tilmes et al.*, 2020]. This experiment follows the SSP5-35-OS overshoot greenhouse gas concentration scenario, and also requires a gradual increase of sulfur injections to keep temperatures at 2020 conditions and a decrease in injections towards the end of the century. However, despite the gradual increase in sulfur injections and stratospheric sulfate burden, *Tilmes et al.* [2020] have noticed an strong reduction in TCO after the onset of sulfur injections for the Southern Hemisphere (SH) ozone hole. This effect was identified for two different starting points of the intervention, in 2020, as well as in 2034.

Recent studies have also suggested that TCO changes as the result of climate intervention using stratospheric sulfur injection are dependent on the injection location. *Kravitz et al.* [2019] investigated differences between the four-point injection strategy used in GLENS and injections at the Equator only. Differences between these injection strategies result in changes in the stratospheric sulfate distributions, radiative heating, strength of the polar vortex, as well as water vapor concentration, which are expected to also change stratospheric ozone. In addition, *Tilmes et al.* [2018a] showed that the effect of stratospheric aerosol interventions on ozone depends on the altitude location of the injections. Furthermore, seasonally varying injections can change the impacts of SAI, for instance on ozone [*Visioni et al.*, 2019]. Finally, we expect that the sensitivity of the ozone response to stratospheric aerosol interventions is also model dependent [*Pitari et al.*, 2014]. So far, no study has investigated the ozone response to these various different factors.

Here, we use four different model experiments that are based on the future unmitigated greenhouse gas forcing scenario RCP8.5. Sulfur injections are determined by the same feedback control algorithm as used in GLENS to keep global surface temperature at 2020 conditions. Three of these experiments are based on the same Earth system model

version but use different injection strategies. One additional experiment has been performed using a different model setup, with higher vertical model resolution. We quantify and discuss the effects of these different experiments on column ozone for an earlier period (2030–39) and a later period (2080–2089) compared to present day (2010–2019). We further explore the cause of the abrupt decrease in column ozone during the onset of stratospheric sulfur injection, especially during the Antarctic ozone hole period.

2 Experimental Design

Simulations were conducted with the state-of-the-art Community Earth System Model, version 1 [*Hurrell et al.*, 2013] with the Whole Atmosphere Community Climate Model CESM1(WACCM) as its atmospheric component. WACCM uses a 0.9° latitude × 1.25° longitude grid. The model includes comprehensive, fully interactive middle atmosphere chemistry with 95 solution species, two invariant species, 91 photolysis reactions, and 207 other reactions. The chemical scheme includes gas-phase and heterogeneous reactions important for stratospheric ozone chemistry, as well as sulfur-bearing gases important for stratospheric sulfate formation [*Mills et al.*, 2017]. A simplified chemistry scheme is used in the troposphere, which supports the formation of aerosols and is coupled to interactive biogenic emissions from the land model. Three of the model experiments use the standard WACCM version with 70 vertical layers (70L), while one uses a higher vertical resolution version with 110 vertical levels (110L) [*Garcia and Richter*, 2019], both reaching up to 150 km ($\approx 10^{-6}$ hPa).

All of the model experiments follow the unmitigated RCP8.5 baseline future concentration pathway. A control RCP8.5 simulation has been performed for both the 70L and 110L WACCM versions. All of the sulfur injection experiments are performed for the period between the years 2020 and 2100 and they include annual sulfur injections that are adjusted with a feedback controller [*MacMartin et al.*, 2017] in order to maintain 2020 global surface temperatures (Table 1). The WACCM experiments using 70 vertical layers include a) results from the geoengineering large ensemble (GLENS) simulations [*Tilmes et al.*, 2018b], with stratospheric point injections at 15°N, 15°S, and 30°N, 30°S, ≈ 6 km above the tropopause with 20 ensemble members; b) and ensemble of 3 simulations of low-altitude (Low) stratospheric point injections at 15°N, 15°S, and 30°N, 30°S ≈ 1 km above the tropopause, and c) an ensemble of 3 simulations of stratospheric point injections at the Equator (EQ) ≈ 6 km above the tropopause. The WACCM 110L

Table 1. CESM WACCM5.4 model experiments with 0.9° × 1.25° horizontal resolution and a model top at ≈ 150km

Experiment	Ensemble Members	Vertical Levels	Injection Latitudes	Injection Altitude above Tropopause
RCP8.5	3	70		
RCP8.5 110L	1	110		
GLENS	20	70	15°N, 15°S, 30°N, 30°S	≈6 km
EQ	3	70	Equator	≈6 km
Low	3	70	15°N, 15°S, 30°N, 30°S	≈1 km
100L	1	110	15°N, 15°S, 30°N, 30°S	≈6 km

experiment (110L) follows the setup of case a), but with only 1 ensemble member. Global, interhemispheric and pole-to equator surface temperatures have been maintained at 2020 conditions (Fig. S-1), except for the EQ case which does not maintain the equator-to-pole gradient. The 110L experiment shows somewhat less warming in the RPC8.5 scenario, which may be a result of reduced stratospheric water vapor in this model configuration [*Wang et al.*, 2018].

3 Results

Stratospheric sulfate distributions for the four performed experiments are very different (Fig. 1, panels a to d). For high-altitude injections, the enhanced sulfate aerosol burden is extended into higher altitudes compared to the low-altitude injections. The EQ case shows the largest burden in the tropics, while the other 70L experiments show larger burdens in the Northern Hemisphere (NH). In contrast, the 110L experiment shows a more equal distribution between the hemispheres (Fig. 1, panel c). The increase in SO_4 burden with time is approximately linear, with largest burdens for the EQ case and lowest burden for the 110L case. The injection rate (Fig. 1, panel f) differs between the four considered cases with largest annual injections for the low case, primarily as a result of faster removal of gases and aerosols with injections closer to the tropopause. For the high-altitude injection experiments, the EQ requires the largest injection rates (up to 60 Tg SO_2 per year by the end of the century), because of a faster removal of larger particles

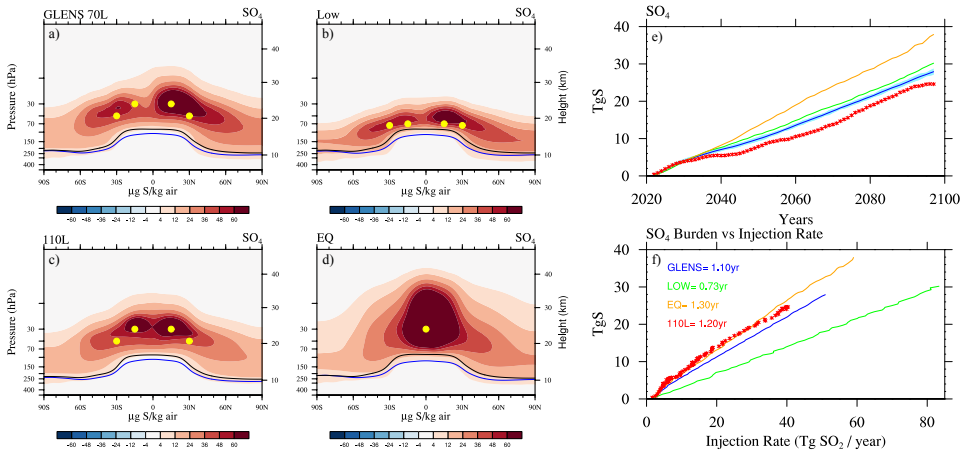

Figure 1. Left panel a-d: Difference of zonally and annually averaged sulfate burden between the ensemble average of stratospheric sulfur injection cases in 2070–2089 and the control experiment for the same period for GLENS (a), Low (b), 110L (c) and EQ (d). The lapse rate tropopause is indicated as a black line for the control and a blue line for the SO_2 injection cases. Yellow dots indicate locations of injection. Right panel e-f: Annual averaged stratospheric sulfate aerosol burden in TgS for the sulfur injection experiments minus the control with time (e) and with injection rate (f). The stratospheric burden vs. injection amount (in unit years) is listed in the panel f for all ensemble members of each experiment.

in the tropical regions compared to the other cases (Fig. S-2). Both Low and EQ experiments further show larger increases in stratospheric water vapor than the other cases, which will lead to more tropospheric warming to be countered by additional injections. The lowest injection rates are needed for the 110L case, possibly because of the reduced stratosphere-troposphere exchange as the result of a better resolved tracer gradient across the tropopause in the 110L model [*von Hobe et al.*, 2021]. Furthermore, the 110L control simulation shows less increase in surface temperature, which may require less sulfur injections to maintain 2020 surface temperature conditions.

Changes in stratospheric ozone as the result of the increasing stratospheric sulfate aerosol burden between 2020 and 2100 differ with region and season, as shown for GLENS (Fig. S-3). The radiative heating of the tropical lower stratosphere results in a warming of the tropical lower stratosphere and an increase of the tropical cold point temperature. This further causes an increase in stratospheric water vapor and a strengthening of the winter polar vortex [e.g., *Richter et al.*, 2017; *Kravitz et al.*, 2019], as well as in-

creases in the vertical velocity above the injection points and increased horizontal transport of tracers towards the poles [*Tilmes et al.*, 2018a]. In addition, the enhanced sulfate mass results in an increase in surface area density (SAD) of aerosols, which, in addition to changes in water vapor and temperature, results in changes in the net photochemical production of ozone through changes (increase and decrease) in different catalytic ozone-destroying cycles. Net chemical production rate changes are also dependent on changes in stratospheric halogen and nitrogen between 2020 and 2100.

In the polar lower stratosphere, halogen and hydrogen are the dominant ozone destroying cycles. These cycles are accelerated due to the enhanced SAD with sulfur injections and result in a reduction of net chemical ozone production rates (defined as the differences between chemical production and loss) [e.g., *Tilmes et al.*, 2009, 2018a]. A reduction in the nitrogen cycle with enhanced SAD is dominant in the polar mid-stratosphere (around 25 km) (see below). Furthermore, the hydrogen cycle is important in the upper stratosphere, where the increase in stratospheric water vapor results in a reduction of net chemical ozone production rates. In mid-latitudes and tropics in the mid-stratosphere, the nitrogen cycle is the most important ozone destroying cycles. The increase in SAD leads to a reduction of reactive nitrogen via hydrolysis of dinitrogen pentoxide [e.g., *Fahey et al.*, 1993] and therefore an increase in net chemical ozone production rates. Combined changes in chemistry and vertical and horizontal transport result in changes of stratospheric ozone and therefore of total column ozone (TCO).

The slow phase-in of sulfur injections in GLENS results in an abrupt reduction in TCO during the ozone hole period in October over Antarctica within the first 10 years of the start of the injection (Fig. 2a). Thereafter, TCO in GLENS remains around 60–70 DU below the values of the control simulation (as further discussed below). Reductions of column ozone over the NH high latitudes in spring are noticeable but smaller (Fig. 2b) compared to the SH, given the larger variability and dynamical influence in the NH. There are no significant changes in TCO after 2070 compared to the control simulation over the Arctic, and both the control and the injection experiments show a significant increase in TCO by the end of the 21st century. January averages over 40–60°N and over the tropics (20°S–20°N) (Fig. 2c,d) also show a significant increase in TCO in the RCP8.5 control experiment by the end of the 21st century. In these regions, increasing SAD due to sulfur injections leads to an increase of TCO compared to the control simulation, which is a result of both, an increase in net ozone production in the trop-

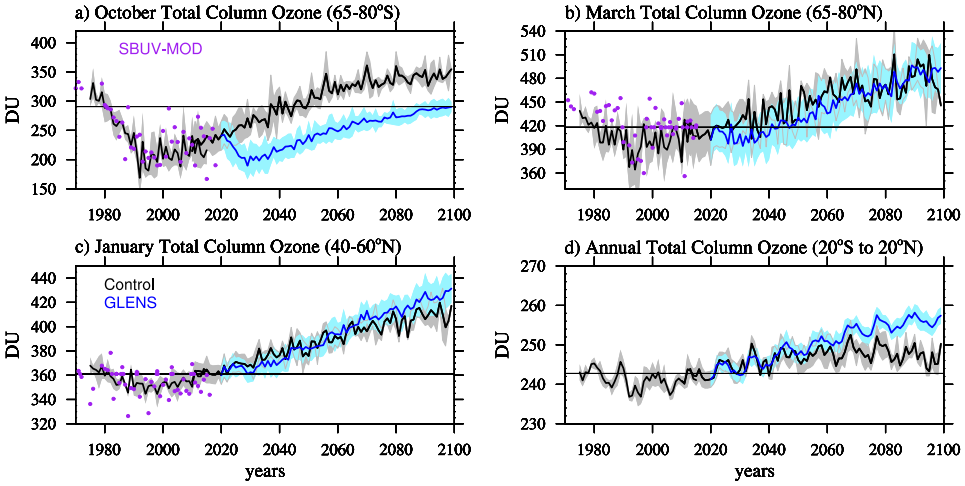

Figure 2. Ensemble average of total column ozone for selected and regions and seasons for the control simulations betweeen 1975-2015 and the future RCP8.5 experiment between 2015 and 2100, based on three ensemble members (black) with standard deviation (grey shaded area), 20 GLENS ensemble members between 2020 and 2100 (blue) with standard deviation (light blue shaded area), and total ozone observations from the Solar Backscatter Ultraviolet (SBUV) Merged Ozone Data (MOD) set (purple symbols). The thin black lines in each panel indicate 1980 conditions.

ics and changes in vertical and horizontal advection [e.g., *Tilmes et al.*, 2018a]. For the four injection experiments, ozone changes are similar in terms of general changes in ozone destroying cyles and dynamical response, and rather differ in magnitude depending on the details of the altered aerosol burden and SAD destribution (Figs. S-4–7).

TCO changes of different sulfur injection experiments in March and October between 2030–2039 and 2010-2019 differ in magnitude and, especially for high latitudes, in sign from the changes between 2080–2089 and 2010-2019 (Fig. 3). These changes are also different from the Control experiment for the same period (Fig. 3 black lines). For the low-altitude injection experiment, to reach a similar sulfate burden as in GLENS, an additional 50% injection rate per year compared to GLENS is required (Fig. 1f). The resulting aerosol distribution is concentrated closer to the tropopause region. This causes more constrained heating at lower altitudes compared to GLENS and a stronger increase in water vapor and thus an increase in the HO_x-ozone destroying cycle, especially pronounced towards the end of the century (Fig. S-5 vs. Fig. S-4). On the other hand, stronger transport of ozone in the low-altitude case from the tropics to the mid- and high lati-

tudes counters the larger reduction of net chemical ozone production rates [*Tilmes et al.*, 2018a]. The low-altitude case therefore shows the lowest decline in TCO in the SH polar region spring of less than 8% (Fig. 3c) and the largest increase in TCO in the NH polar region spring in 2080–2089 of up to 20% compared to 2010–2019 (Fig. 3b).

The equatorial injection case requires an $\approx$ 10% larger injection rate per year than GLENS. About a 35% larger burden is confined in the tropics and reaches towards higher altitudes than the GLENS experiment (Fig. 1). This results in increased radiative heating of the tropopause and with that in even larger increases in water vapor compared to GLENS and Low, and more pronounced changes in the HO_x cycle. The equatorial injections further result in a stronger confinement of air masses in the tropical pipe [*Niemeier and Schmidt*, 2017; *Visioni et al.*, 2020; *Kravitz et al.*, 2019] and a stronger and colder polar vortex. Increases in ozone destroying catalytic cycles and reduced horizontal transport result in the slowest TCO recovery during SH spring towards the end of the century compared to the other experiments (Fig. 3, Fig. 4b) and also results in larger increases in NH mid-latitude TCO in January (Fig. S-8).

The 110L experiment requires $\approx$ 30% less sulfur injections to reach the same temperature targets as GLENS (Fig. 1f), resulting also in a smaller SAD compared to the other experiments, until about 2070. Afterwards, SAD in the 110L experiment is indicating a steeper increase. The increase in stratospheric water vapor and therefore the effects on the ozone destroying HO_x cycle are comparable to GLENS (Figs. S-4 and S-5). The more evenly distributed aerosol burden between the hemispheres results in a shift of the net chemical production rate through the reduced NO_x cycle from the NH towards the SH and a more equal change in ozone in the tropical lower stratosphere (Fig. S-7). In this experiment, effects on the SH polar vortex are smaller compared to GLENS, while there is a faster recovery of TCO towards in 2080-2089 compared to 2010-19 (Fig. 3).

In contrast to the sulfur injection experiments, the Control experiment shows a positive change (recovery) of TCO between 2030–2039 and 2010–2019, in particular for high polar latitudes in spring of each hemisphere. Differences between the climate intervention and the Control experiment for changes in TCO between 2080-89 and 2010-2019 show the same sign, however are smaller for the NH mid-and high latitudes, while larger for the SH polar region.

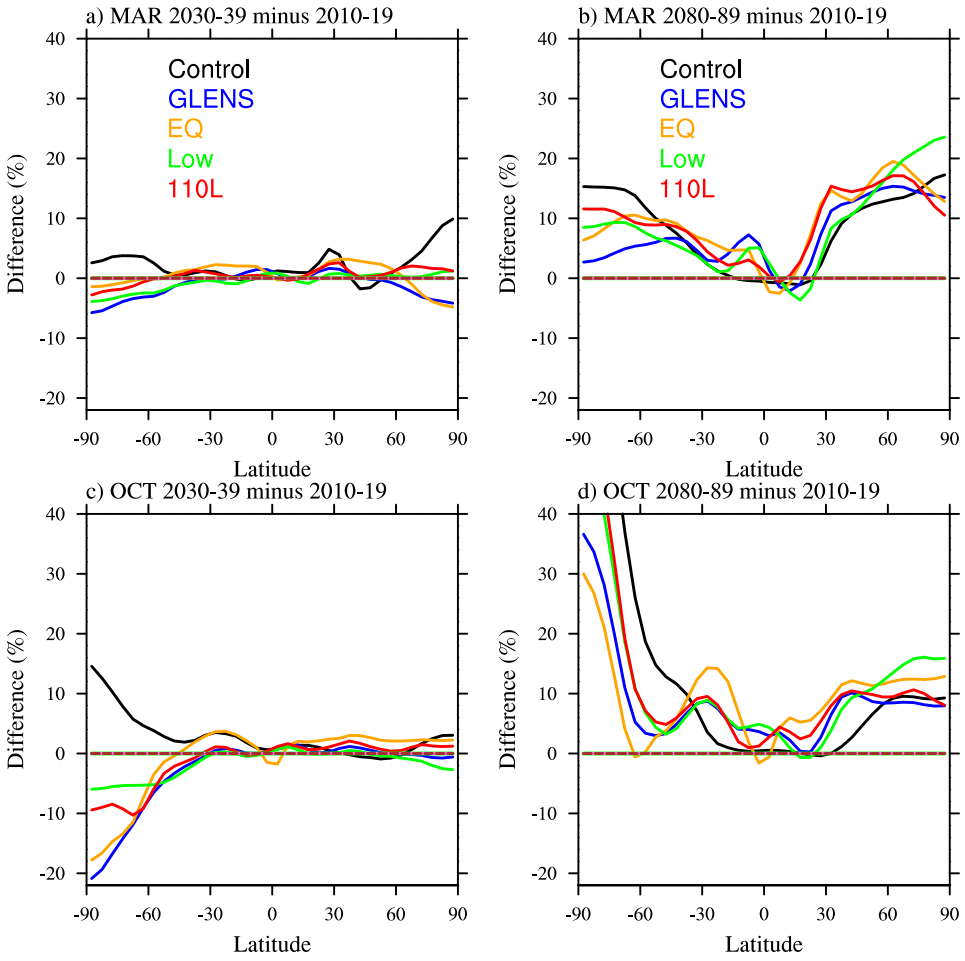

Figure 3. Relative differences of zonal averaged total column ozone between 2030–2039 and 2010–2019 (panels a and c) and 2080–2089 and 2010–2019 (panels b and d) for March (top) and October (bottom) for the different experiments (different colored lines).

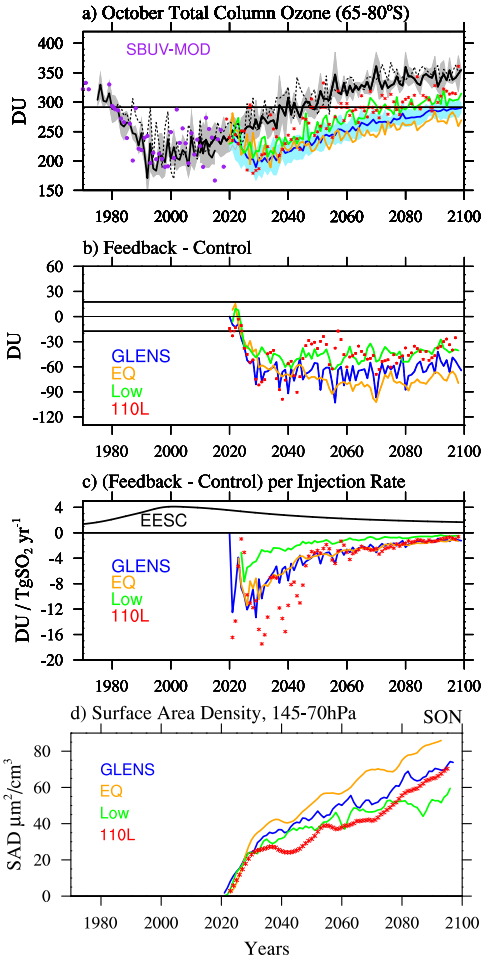

Figure 4. Panel a): October averaged total column ozone between 65 and 80°S (see Fig. 2a) for additional model experiments (different colors). Solid lines represent ensemble averages of the different experiments. Grey and light blue areas show the standard deviation of the GLENS ensemble and the thin black line indicates 1980 conditions. Red stars show a 3-year running mean of the one ensemble of the 110L experiment. Total column ozone observations from the Solar Backscatter Ultraviolet (SBUV) Merged Ozone Data (MOD) set are shown as purple symbols. Panel b): Differences of column ozone between sulfur injection experiments and corresponding baseline experiments; the two black lines around zero indicate the standard deviation from the GLENS baseline simulations. A running mean over 3 years has been applied to the results. Panel c): Column ozone difference per sulfur injection per year. Black thick line indicates the evolution of Effective Equivalent Stratospheric Chlorine (EESC) amount for the polar regions. Panel d) Zonal averaged Surface Area density between 65 and 90°S and 70–145 hPa altitude for September/October/November.

The Antarctic October TCO evolution in both control simulations, WACCM 70L and WACCM 110L, follows the observed decline between 1980 and 2000 (Fig. 4a). After the minimum has been reached in the model around year 1990–2000, TCO increases (following RCP8.5) until reaching 1980 conditions around 2045. The super recovery (above 1980 values) is caused by a speed-up of the stratospheric Brewer-Dobson circulation, as well as by a cooling of stratospheric temperatures with increasing greenhouse gases, which reduces gas-phase ozone production in the upper stratosphere [*Butler et al.*, 2016]. Despite the differences in injection strategies, all four experiments show an abrupt decrease in column ozone in the first 10 years after the start of the injections. Afterwards, differences between the sulfur injection experiments and the control simulations stay approximately constant with $\approx$ 40–50 DU reductions for the Low and 110L case, 60–70 DU for GLENS, and around 80 DU for the EQ experiment (Fig. 4b). The recovery of the ozone hole to 1980 conditions is therefore delayed by 20–30 years for the Low and 110L case and $\approx$ 55 years for GLENS. The EQ experiment does not show a recovery by the end of the 21st century.

The strong decline in TCO in the first 10 years of the start of the injections can be understood by illustrating TCO changes per injection amount in comparison to changes in the effective equivalent stratospheric chlorine (Fig. 4c) and surface area density (Fig. 4d) in the polar lower stratosphere. Reductions TCO per injection amount reach maximum values during the first 10 years of the start of the injections and show a strong decline thereafter. The equivalent effective stratospheric chlorine (EESC) content is decaying almost linearly after 2020 and can therefore not be responsible for the strong initial decline of TCO. On the other hand, surface area density shows a strong increase in the first 10 years and then changes to a moderate increase in 2030, while the increase in sulfate mass per year is about constant. This is aligned with the increase in effective radius in the polar regions, which is almost the same for all the four injection experiments (Fig. S-2). The effective radius in the SH polar region in SON requires up to 10 years to reach $\approx$ 0.4 microns. After that, it grows about 0.03 micron per 10 years. The initial small injection amounts result in relatively larger SAD compared to larger injection amounts and are therefore much more efficient in destroying ozone.

4 Summary

The rate of change of TCO caused by stratospheric sulfur injections in the SH polar region during October is largest within 10 years after the start of the injection experiments. These relatively abrupt changes, as the result of a sharp increase in SAD and effective radius, result in a decrease of TCO between 8% and 20% in 2030–39 compared to 2010–2019, depending on the injection strategy and model version. Smaller changes of ±5% are simulated for other regions and seasons. The onset of stratospheric aerosol intervention using sulfate aerosols is therefore expected to result in an abrupt decline of SH October TCO. *Tilmes et al.* [2020] have also shown declines of similar magnitude in SH polar ozone assuming a later start of injections in 2034, a time when the chlorine burden is reduced.

After about 2030, the continuous increase of SH polar TCO following the non-mitigated RCP8.5 control simulation dominates the trend in column ozone with or without stratospheric sulfur injection between 2030 and 2100. In the SH polar vortex, TCO recovers in all scenarios towards the end of the century, except for the EQ injection case, which is likely to recover a few years later. The ozone hole recovery to 1980 conditions is however delayed for about 25 years for the low-altitude and the 110L experiment and ≈ 55 years for GLENS. In the NH polar vortex in spring, initial small reductions of less than 5% in TCO between 2030-39 and 2010-19 are reversed with an increase in TCO of up to 20% depending on the scenario between 2010–19 and 2080–89. Stratospheric aerosol interventions would increase TCO by 10–20 DU in tropics and mid latitudes towards the end of the century compared to the Control for the same period, with some changes depending on the injection experiment. Theses results are based on continously increasing sulfur injections towards the end of the 21st century. In case of a different greenhouse gas emission scenario with SAI using declining sulfur injections in the second half of the 21st century, the delay of the ozone hole recovery may be shortened by 20–30 years [*Tilmes et al.*, 2020].

For this analysis monthly and zonal mean TCO changes have been investigated. We have not considered regional and daily extremes that could be much larger, for example for cold Arctic winters [*Tilmes et al.*, 2008]. Further in-depth analyses have to be performed to identify processes that result in the TCO changes, in particular over the SH and NH high latitudes and within the polar vortex. Effects of TCO changes on sur-

face UV have not yet been investigated. Impact assessments, for instance of UV changes on ecosystems may need to take into account changes and trends starting from the present-day conditions in order to project impacts of potential future changes in TCO. To support these analyses, we have chosen to present ozone changes relative to present-day conditions (2010–19) (see Fig. 3). Finally, results in this study are based on two configurations of one model with somewhat different outcomes, in particular with regard to the aerosol distribution. Experiments of the different injection scenarios have to be investigated in a multi-model context using multiple ensemble members, in order to understand the range of outcomes and uncertainties.

Acknowledgments

We thank Gary Strand and Ilana Stern, for publishing the model output on the NCAR Earth System Grid and Alice Bertini offering software support in producing diagnostics for model results. Support for Ben Kravitz was provided in part by the National Science Foundation through agreement CBET-1931641, the Indiana University Environmental Resilience Institute, and the Prepared for Environmental Change Grand Challenge initiative. The Pacific Northwest National Laboratory is operated for the US Department of Energy by Battelle Memorial Institute under contract DE-AC05-76RL01830. The CESM project is supported primarily by the National Science Foundation. This material is based upon work supported by the National Center for Atmospheric Research, which is a major facility sponsored by the NSF under Cooperative Agreement No. 1852977. Computing and data storage resources, including the Cheyenne supercomputer (doi:10.5065/D6RX99HX), were provided by the Computational and Information Systems Laboratory (CISL) at NCAR. This research was developed with funding from the Defense Advanced Research Projects Agency (DARPA). The views, opinions, and/or findings expressed are those of the authors and should not be interpreted as representing the official views or policies of the Department of Defense or the U.S. Government. All simulations were carried out on the Cheyenne high-performance computing platform https://www2.cisl.ucar.edu/user-support/acknowledging-ncarcisl, and are available to the community via the Earth System Grid (see information at http://www.cesm.ucar.edu/projects/community-projects/GLENS/).

References

Butler, A. H., J. S. Daniel, R. W. Portmann, A. R. Ravishankara, P. J. Young, D. W. Fahey, and K. H. Rosenlof (2016), Diverse policy implications for future ozone and surface UV in a changing climate, *Environmental Research Letters*, *11*(6), 064,017, doi:10.1088/1748-9326/11/6/064017.

Fahey, D., S. Kawa, E. Woodbridge, P. Tin, J. Wilson, H. Jonsson, J. Dye, D. Baumgardner, S. Borrmann, and D. Toohey (1993), In situ measurements constraining the role of sulphate aerosols in mid-latitude ozone depletion, *Nature*, *363*, 509–514.

Garcia, R. R., and J. H. Richter (2019), On the Momentum Budget of the Quasi-Biennial Oscillation in the Whole Atmosphere Community Climate Model, *Journal of the Atmospheric Sciences*, *76*(1), 69–87, doi:10.1175/JAS-D-18-0088.1.

Heckendorn, P., D. Weisenstein, S. Fueglistaler, B. P. Luo, E. Rozanov, M. Schraner, L. W. Thomason, and T. Peter (2009), The impact of geoengineering aerosols on stratospheric temperature and ozone, *Environmental Research Letters*, *4*, 045,108, doi:10.1088/1748-9326/4/4/045108.

Hurrell, J. W., H. M. M., P. R. Gent, S. Ghan, J. E. Kay, P. H. Kushner, J.-F. Lamarque, W. G. Large, D. Lawrence, L. K., W. H. Lipscomb, C. L. M, N. Manhowald, D. R. Marsh, R. B. Beale, P. Rasch, S. Vavrus, M. Verteinstein, D. Bader, W. D. Collins, J. J. Hack, J. Kiehl, and S. Marshall (2013), A Framework for Collaborative Research, *B. Am. Meteorol. Soc.*, *94*(November 2012), 1339–1360, doi:10.1175. BAMS-D-12-00121.1.

Kravitz, B., D. G. MacMartin, M. J. Mills, J. H. Richter, S. Tilmes, J.-F. Lamarque, J. J. Tribbia, and F. Vitt (2017), First Simulations of Designing Stratospheric Sulfate Aerosol Geoengineering to Meet Multiple Simultaneous Climate Objectives, *Journal of Geophysical Research: Atmospheres*, *122*(23), doi:10.1002/2017JD026874.

Kravitz, B., D. G. MacMartin, S. Tilmes, J. H. Richter, M. J. Mills, W. Cheng, K. Dagon, A. S. Glanville, J. Lamarque, I. R. Simpson, J. Tribbia, and F. Vitt (2019), Comparing Surface and Stratospheric Impacts of Geoengineering With Different SO_2 Injection Strategies, *Journal of Geophysical Research: Atmospheres*, *124*(14), 7900–7918, doi:10.1029/2019JD030329.

MacMartin, D. G., B. Kravitz, S. Tilmes, J. H. Richter, M. J. Mills, J.-F. Lamarque, J. J. Tribbia, and F. Vitt (2017), The Climate Response to Stratospheric Aerosol Geoengineering Can Be Tailored Using Multiple Injection Locations, *Journal of Geophysical Research: Atmospheres*, *122*(23), doi:10.1002/2017JD026868.

Mills, M. J., J. H. Richter, S. Tilmes, B. Kravitz, D. G. MacMartin, A. A. Glanville, J. J. Tribbia, J.-F. Lamarque, F. Vitt, A. Schmidt, A. Gettelman, C. Hannay, J. T. Bacmeister, and D. E. Kinnison (2017), Radiative and chemical response to interactive stratospheric sulfate aerosols in fully coupled CESM1(WACCM), *Journal of Geophysical Research: Atmospheres*, *122*(23), doi:10.1002/2017JD027006.

Niemeier, U., and H. Schmidt (2017), Changing transport processes in the stratosphere by radiative heating of sulfate aerosols, *Atmospheric Chemistry and Physics*, *17*(24), 14,871–14,886, doi:10.5194/acp-17-14871-2017.

Pitari, G., V. Aquila, B. Kravitz, A. Robock, S. Watanabe, I. Cionni, N. D. Luca, G. D. Genova, E. Mancini, and S. Tilmes (2014), Stratospheric ozone response to sulfate geoengineering: Results from the Geoengineering Model Intercomparison Project (GeoMIP), *Journal of Geophysical Research: Atmospheres*, *119*(5), 2629–2653, doi:10.1002/2013JD020566.

Rasch, P. J., S. Tilmes, R. P. Turco, A. Robock, L. Oman, C.-C. Chen, G. L. Stenchikov, and R. R. Garcia (2008), An overview of geoengineering of climate using stratospheric sulphate aerosols, *Philosophical transactions. Series A, Mathematical, physical, and engineering sciences*, *366*(1882), 4007–37, doi:10.1098/rsta.2008.0131.

Richter, J. H., S. Tilmes, M. J. Mills, J. J. Tribbia, B. Kravitz, D. G. MacMartin, F. Vitt, and J. F. Lamarque (2017), Stratospheric Dynamical Response to SOO_2 Injections, *Journal of Geophysical Research Atmospheres*, *122*(23).

Tilmes, S., R. Müller, and R. Salawitch (2008), The sensitivity of polar ozone depletion to proposed geoengineering schemes., *Science*, *320*(5880), 1201–1204, doi:10.1126/science.1153966.

Tilmes, S., R. R. Garcia, D. E. Kinnison, A. Gettelman, and P. J. Rasch (2009), Impact of geoengineered aerosols on the troposphere and stratosphere, *Journal of Geophysical Research*, *114*(D12), D12,305, doi:10.1029/2008JD011420.

Tilmes, S., D. E. Kinnison, R. R. Garcia, R. Salawitch, T. Canty, J. Lee-Taylor, S. Madronich, and K. Chance (2012), Impact of very short-lived halogens on

stratospheric ozone abundance and UV radiation in a geo-engineered atmosphere, *Atmospheric Chemistry and Physics*, *12*(22), 10,945–10,955, doi:10.5194/acp-12-10945-2012.

Tilmes, S., J. H. Richter, M. J. Mills, B. Kravitz, D. G. MacMartin, R. R. Garcia, D. E. Kinnison, J. Lamarque, J. Tribbia, and F. Vitt (2018a), Effects of Different Stratospheric SOO_2 Injection Altitudes on Stratospheric Chemistry and Dynamics, *Journal of Geophysical Research: Atmospheres*, *123*(9), 4654–4673, doi:10.1002/2017JD028146.

Tilmes, S., J. H. Richter, B. Kravitz, D. G. MacMartin, M. J. Mills, I. R. Simpson, A. S. Glanville, J. T. Fasullo, A. S. Phillips, J.-F. Lamarque, J. Tribbia, J. Edwards, S. Mickelson, and S. Ghosh (2018b), CESM1(WACCM) Stratospheric Aerosol Geoengineering Large Ensemble Project, *Bulletin of the American Meteorological Society*, *99*(11), 2361–2371, doi:10.1175/BAMS-D-17-0267.1.

Tilmes, S., D. G. MacMartin, J. T. M. Lenaerts, L. van Kampenhout, L. Muntjewerf, L. Xia, C. S. Harrison, K. M. Krumhardt, M. J. Mills, B. Kravitz, and A. Robock (2020), Reaching 1.5 and 2.0C global surface temperature targets using stratospheric aerosol geoengineering, *Earth System Dynamics*, *11*(3), 579–601, doi:10.5194/esd-11-579-2020.

Visioni, D., D. G. MacMartin, B. Kravitz, S. Tilmes, M. J. Mills, J. H. Richter, and M. P. Boudreau (2019), Seasonal Injection Strategies for Stratospheric Aerosol Geoengineering, *Geophysical Research Letters*, *46*(13), 7790–7799, doi:10.1029/2019GL083680.

Visioni, D., D. G. MacMartin, B. Kravitz, W. Lee, I. R. Simpson, and J. H. Richter (2020), Reduced Poleward Transport Due to Stratospheric Heating Under Stratospheric Aerosols Geoengineering, *Geophysical Research Letters*, *47*(17), doi:10.1029/2020GL089470.

von Hobe, M., F. Ploeger, P. Konopka, C. Kloss, A. Ulanowski, V. Yushkov, F. Ravegnani, C. M. Volk, L. L. Pan, S. B. Honomichl, S. Tilmes, D. E. Kinnison, R. R. Garcia, and J. S. Wright (2021), Upward transport into and within the Asian monsoon anticyclone as inferred from StratoClim trace gas observations, *Atmospheric Chemistry and Physics*, *21*(2), 1267–1285, doi:10.5194/acp-21-1267-2021.

Wang, X., Y. Wu, W.-W. Tung, J. H. Richter, A. A. Glanville, S. Tilmes, C. Orbe, Y. Huang, Y. Xia, and D. E. Kinnison (2018), The Simulation of Stratospheric Water Vapor Over the Asian Summer Monsoon in CESM1(WACCM) Models, *Journal of Geophysical Research: Atmospheres*, *123*(20), 11,377–11,391, doi: 10.1029/2018JD028971.

Xia, L., P. J. Nowack, S. Tilmes, and A. Robock (2017), Impacts of stratospheric sulfate geoengineering on tropospheric ozone, *Atmospheric Chemistry and Physics*, *17*(19), 11,913–11,928, doi:10.5194/acp-17-11913-2017.